Journal of
Computational and Theoretical Nanoscience
Vol. 6, 1–12, 2009

Influence of Band Non-Parabolicity on Few Ballistic Properties of III–V Quantum Wire Field Effect Transistors Under Strong Inversion

Sitangshu Bhattacharya* and Santanu Mahapatra

Nanoscale Device Research Laboratory, Centre for Electronics Design and Technology, Indian Institute of Science, Bangalore 560012, India

A simplified analytical approach on few ballistic properties of III–V quantum wire transistor has been presented by considering the band non-parabolicity of the electrons in accordance with Kane's energy band model using the Bohr-Sommerfeld's technique. The confinement of the electrons in the vertical and lateral directions are modeled by an infinite triangular and square well potentials respectively, giving rise to a two dimensional electron confinement. It has been shown that the quantum gate capacitance, the drain currents and the channel conductance in such systems are oscillatory functions of the applied gate and drain voltages at the strong inversion regime. The formation of subbands due to the electrical and structural quantization leads to the discreetness in the characteristics of such 1D ballistic transistors. A comparison has also been sought out between the self-consistent solution of the Poisson's-Schrödinger's equations using numerical techniques and analytical results using Bohr-Sommerfeld's method. The results as derived in this paper for the all the energy band models gets simplified to the well known results under certain limiting conditions which forms the mathematical compatibility of our generalized theoretical formalism.

Keywords: 1DEG, Ballistic Properties, Quantized Gate Capacitances, III–V, Density-of-States.

RESEARCH ARTICLE

1. INTRODUCTION

Rapid downscaling in device dimension has generated a plethora of interesting applications.[1] The two dimensional carrier transport encountered in hetero-structured devices, due to the reduction of the carrier propagation vector along one direction, leads to the generation of quantized energy levels, allowing a 2D carrier transport phenomena which, dramatically affects the working principles of such devices and, cannot be explained by using classical methods. The carrier transport in the so-called quantum wire field effect transistors (QWFETs) allows a further increment in the carrier confinement, giving rise to a two sets of quantum numbers, resulting in wide variation at the performance level as compared with their corresponding 2D and bulk structural systems. Recent challenges, as predicted by International Roadmap for Semiconductors[2] (ITRS), indicates that the incorporation of III–V semiconductors as channel materials is one of the vital issues from both theoretical and fabrication point of view over the past few years. QWFETs like InGaAs/InAs,[3] AlGaAs/GaAs,[4] InAs/InP,[5] etc. have been extensively fabricated for increasing the drive current capability and large trans-conductance.[1] The mode of carrier transport in nanoscale transistors are mainly due to their ballistic mechanisms[6] which devoid the incorporation of scattering, at least at low temperatures. Selective doping in such systems readily removes the ionized impurity scattering. Recent developments suggest that the ballistic nature has an appreciable amount of contribution, even at 50 nm range devices.[7] Experimental evidences recommend that the drain current and conductance in such QWFETs are oscillatory functions of gate and drain voltages.[3, 8, 9]

In this paper, we present a simplified yet analytical approach using the Bohr-Sommerfeld's technique to determine the 1D density of states, number of subbands, the quantum gate capacitance and the drive current for ballistic QWFETs whose channel electrons obeys the non-parabolic dispersion relations modeled by Kane.[10–12] The technique is based on the modified Thomas-Fermi approximation (MTFA).[12–21] Recently[22], good agreement has been found between the analytical and numerical solutions by using MTFA and Poisson's-Schrödinger's equations for the band bending, charge profiles and the subbands by incorporating

*Author to whom correspondence should be addressed.

Kane's second order non-parabolic dispersion relation for carriers in a 2D quantized accumulation layers. It has also shown by the authors,[23] that a nearly complete 2D subband structure for a third order non-parabolic dispersion relation in inversion layers of δ-doped FETs can be determined by using the same technique.

There are several ways of transforming a 2D electron gas (2DEG) to a 1D electron gas (1DEG). The method generally presented in literature involves the application of an external applied electrical potential, as in the case of tri-gate, strain-induced FETs, etc.[24] However, a 1D electron system can also be created by applying an electrical and a structural confinement.[25] The electrical confinement can be due to a strong electric field at the hetero-structure interface in a vertical direction resulting in a 2D strong inversion layer, while the structural confinement can be due to the a lateral mesa-etching, resulting in a quantum well.[25] For the present case, as shown in Figure 1, we shall approximate the shape of the electrical potential at the interface to be much like a linear triangular well at strong inversion.[26] To incorporate the third order non-parabolicity of Kane, we shall also take the channel material to be InAs, which has a spin-orbit splitting constant in the order of their respective band-gap.[11]

Due to the introduction of band non-parabolicity, the 1D density-of-states (DOS) in such system becomes a function of the electron energy and hence a detailed theoretical study of determination of the characteristic parameters for such ballistic QWFETs will be of much interest to investigate.

What follows, in the theoretical background, we shall formulate the coupled Poisson's-Schrödinger's equation for the present case and will evaluate the complete energy subbands structure taking the third, second and first order energy band models of Kane numerically for the self-consistency of the solutions, followed by a detailed analytical derivation of the carrier energy dispersion relation in 1DEG QWFETs using Bohr-Sommerfeld's quantization rule.[12–21] The expressions of 1DDOS, carrier degeneracy, threshold voltage, quantum gate capacitance, and finally the drain current for all the energy band models in ballistic III–V QWFETs under the strong inversion regime will be formulated thereafter. We shall also study how all the results for all the energy band model reduces to the well known classical fallouts under certain limiting conditions.

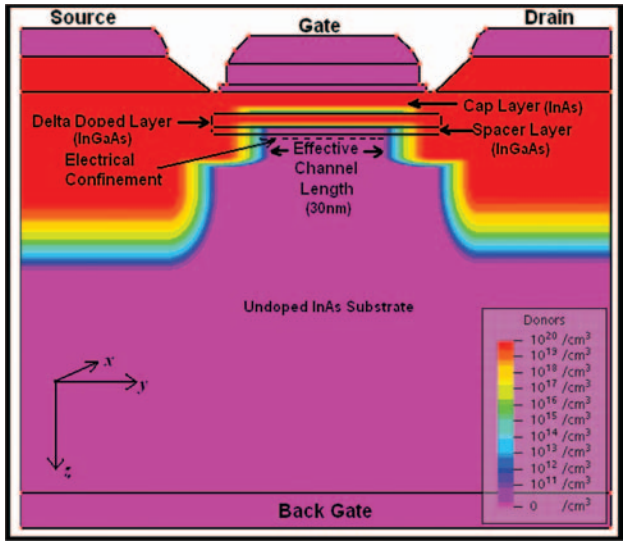

Fig. 1. Doping profile of the donor atoms in delta-doped InGaAs/InAs QWFET. The lateral effective channel dimension has been taken as 20 nm. The thickness of the cap, doped and spacer layer are 10 nm, 5 nm and 5 nm respectively.

2. THEORETICAL BACKGROUND

2.1. Formulation of the Coupled Poisson's-Schrödinger's Solution Using Effective Mass Approximation in the Strong Inversion Regime for the QWFETs, Whose Channel Electrons Obey the Three, Two and the Parabolic Energy Band Model of Kane

Using $\mathbf{k}\cdot\mathbf{p}$ mechanism, the energy eigen-values considering the of the spin-orbit interaction of the electrons following Kane[10–11] can be written as

$$(\in -E_c)(\in -E_v)(\in -E_v+\Delta) - p^2k^2(\in -E_v+2\Delta/3)=0 \quad (1)$$

in which, $\in = E-\hbar^2k^2/2m_0$, E is the energy eigen-value and is measured from the bottom of the conduction band minimum in vertically upward direction, m_0 is the free electron mass, E_c and E_v are the energies corresponding to the conduction band minimum and valance band maximum, p is the momentum matrix element, k is the electron wave vector and Δ is the spin-orbit splitting constant.

Eliminating p, Eq. (1) simplifies as[11]

$$\frac{\hbar^2k^2}{2m^*}\left(1-\frac{m^*}{m_0}\right) = \in\left[\frac{(E_g+2\Delta/3)}{E_g(E_g+\Delta)}\frac{(\in +E_g)(\in +E_g+\Delta)}{(\in +E_g+2\Delta/3)}\right] \quad (2)$$

where, $\hbar(=h/2\pi)$, h is the Planck's constant, m^* is the isotropic effective electron mass at the edge of the conduction band and E_g is the band gap.

It should be noted that analysis of the subband energies determined by taking parabolic energy band models for materials like InAs, InSb, etc. can highly deviate from the actual reality since, at high electric field, the electrons in such materials follows the non-parabolic energy relations. Furthermore, since, the band gap of these compounds is in the order of their spin-orbit splitting constant the analyses can highly be inaccurate for such systems. However, it can theoretically be shown for a self comparison, the deviation of including such energy band models.

Thus, when, $E_g \gg \Delta$ or for low energy electrons, Eq. (2) can be written as

$$\in (1+\alpha \in) = \frac{\hbar^2 k^2}{2m^*}\left(1-\frac{m^*}{m_0}\right) \tag{3}$$

in which, $\alpha = (1/E_g)(1-m^*/m_0)(1-E_g\Delta/(3(E_g+2\Delta/3)(E_g+\Delta)))$ is the non-parabolicity factor.

For electrons following the parabolic energy band model of Kane, Eq. (3) transform to

$$\in = \frac{\hbar^2 k^2}{2m^*}\left(1-\frac{m^*}{m_0}\right) \tag{4}$$

The one electron time independent Schrödinger's equation for a confining potential $V(x,z)$ along the vertical (z-direction) and a lateral (x-direction) can be written as

$$[-\hbar^2/2m^*(\partial^2/\partial x^2+\partial^2/\partial z^2)+V(x,z)]\psi(x,z) = \in \psi(x,z) \tag{5}$$

where, in this case, $\in = E-\hbar^2 k_y^2/2m_0$.

The confining potential $V(x,z)$ can be written as a sum of potential along two directions as

$$V(x,z) = V(x)+V(z) \tag{6}$$

in which

$$V(x) = \begin{cases} 0, & \text{for } 0 \le x \le l_x \\ \infty, & \text{for } x \le 0,\ x \ge l_x \end{cases} \quad \text{and}$$

$$V(z) = \begin{cases} eF_s z, & \text{for } z > 0 \\ \infty, & \text{for } z \le 0 \end{cases}$$

where, l_x, e and F_s are the nanometer thickness along x-direction (lateral), the magnitude of the electronic charge and the surface electric field at the interface pointing along the z-direction (vertically downward).

The normalized solution to Eq. (5) can be written as the product of the individual envelope functions

$$\psi(x,z) = \sum_{n_x=1}^{n_{x\max}}\sum_{i=0}^{i_{\max}}\left\{\sqrt{\frac{2}{l_x}}\sin\left(\frac{n_x\pi}{l_x}\right)\psi_i(z)\right\}\exp(i\vec{k}_\parallel\cdot\vec{r}_\parallel) \tag{7}$$

where,

$$\psi_i(z) = \begin{cases} (a^{1/2}/(A_i(b_i))')A_i(az+b_i), & z > 0 \\ 0, & z < 0 \end{cases}$$

in which, n_x and i are the quantum numbers due to the structural and electrical confinement, A_i are the Airy functions,[27] $a = (2m^*eF_s/\hbar^2)^{1/3}$, $b_i = (-aE_i/eF_s)$, $(A_i(b_i))'$ is the derivative of A_i evaluated at $z=0$ and E_i are the subband energies due to the electrical confinement respectively.

Considering an undoped InAs substrate and a delta-doped InGaAs layer for an InGaAs/InAs QWFET as shown in Figure 1, the related Poisson's equation can be written for the present case as

$$\frac{\partial^2 V(z)}{\partial z^2} = -e^2\left(\frac{N_D(z)}{\varepsilon_d}+\frac{N_c}{\varepsilon_{sc}}+\frac{n_{1D}}{\varepsilon_{sc}}\right) \tag{8}$$

in which, ε_d and ε_{sc} are the permittivity of the δ-doped and the channel permittivity, N_c is the donor density of the cap layer, n_{1D} is the 1D carrier density confined in the channel and a Gaussian distribution of the donor density ($N_D(z)$) following[28] has been taken between the spacer and the cap layer as measured from the interface.

The 1D carrier density can be expressed following[29] as

$$n_{1D} = \sum_{n_x=1}^{n_{x\max}}\sum_{i=0}^{i_{\max}}\left[\left\{\int \frac{1}{2\pi^2}\left[1+\exp\left(\frac{E_n+E_i-E_F}{k_B T}\right)\right]^{-1} dk_z\right\} \times |\psi(x,z)|^2\right] \tag{9}$$

where, k_B and T are the Boltzmann's constant and temperature respectively.

The use of Eqs. (7), (8) and (9) can be computed self-consistently to solve for the energy eigen-values for all the band models of Kane under the two confining potentials. The ballistic drain current for ideal contacts in such systems at a low drain voltage can thus be numerically computed using Landauer's formalism[30]

$$I_d = \frac{2g_v e}{h}\sum_{n_x=1}^{n_{x\max}}\sum_{i=0}^{i_{\max}}\int [f(E-E_{F_+})-f(E-E_{F_-})]\,dE \tag{10}$$

in which, g_v is the valley degeneracy, $f(E-E_{F_\pm})$ are the equilibrium distribution function at the source and the drain terminals respectively.

2.2. Formulation of the Electron Dispersion Relation, Quantized Subbands, Density-of-States Function, Carrier Statistics and Quantum Capacitance in Quantum Wire Field Effect Devices Using Bohr-Sommerfeld's Quantization Rule in the Strong Inversion Regime Considering the Third, Second and First Order Band Non-Parabolicity

Applying a linear triangular potential-well approximation,[26] the complete electric subband structures parallel to the interface can be written using the Bohr-Sommerfeld's rule[12–21, 23]

$$\int_{z=0}^{z_T} k_z\,dz = \frac{2}{3}(a_i)^{3/2} \tag{11}$$

where z_T is the classical turning point.

Under the application of an external electric field at the surface, Eq. (2) assumes the form

$$\zeta_3(E) - eF_s z[\zeta_3(E)]' = \frac{\hbar^2 k^2}{2m^*} \tag{12}$$

in which, $\zeta_3(E) \equiv (E(E+E_g)(E+E_g+\Delta)(E_g+2\Delta/3))/(E_g(E_g+\Delta)(E+E_g+2\Delta/3)) = \hbar^2 k^2/2m^*$, the primes

RESEARCH ARTICLE

denote the differentiation of the differentiable functions with respect to E, $k^2 = k_s^2 + k_z^2$ and $k_s^2 = k_x^2 + k_y^2$.

Thus, for a two dimensional confinement, Eq. (11) can be written as

$$\int_{z=0}^{z_T} \left[\zeta_3(E) - eF_s z[\zeta_3(E)]' - \left\{\frac{\hbar^2 k_y^2}{2m^*} + \frac{\hbar^2}{2m^*}\left(\frac{n_x\pi}{l_x}\right)^2\right\}\right]^{1/2} dz = \frac{2\hbar}{3\sqrt{2m^*}}(a_i)^{3/2} \quad (13)$$

where

$$z_T = [eF_s[\zeta_3(E)]']^{-1}[\zeta_3(E) - \{\hbar^2 k_y^2/(2m^*) + \hbar^2/(2m^*)(n_x\pi/l_x)^2\}]$$

Eq. (13) leads to the dispersion relation for the 1DEG in III–V QWFETs incorporating the third order non-parabolicity of Kane as

$$\zeta_3(E) - \left\{\frac{\hbar^2}{2m^*}\left(\frac{n_x\pi}{l_x}\right)^2 + a_i\left[\frac{\hbar eF_s[\zeta_3(E)]'}{\sqrt{2m^*}}\right]^{2/3}\right\} = \frac{\hbar^2 k_y^2}{2m^*} \quad (14)$$

The 1D quantized subband energies ($E_{n,i}$) in this case can be written as

$$\zeta_3(E_{n,i}) = \frac{\hbar^2}{2m^*}\left(\frac{n_x\pi}{l_x}\right)^2 + a_i\left[\frac{\hbar eF_s[\zeta_3(E_{n,i})]'}{\sqrt{2m^*}}\right]^{2/3} \quad (15)$$

The 1D total density-of-states function in such system assumes the form

$$N_{1D}(E) = \frac{g_v}{2\pi}\left(\frac{2m^*}{\hbar^2}\right)^{1/2} \sum_{n_x=1}^{n_{x\max}} \sum_{i=0}^{i_{\max}} \left[[\zeta_3(E)]' \left\{\zeta_3(E) - \frac{\hbar^2}{2m^*}\left(\frac{n_x\pi}{l_x}\right)^2 - a_i\left[\frac{\hbar eF_s[\zeta_3(E_{n,i})]'}{\sqrt{2m^*}}\right]^{2/3}\right\}^{-1/2} H(E - E_{n,i})\right] \quad (16)$$

where g_v is the valley degeneracy, H is the Heaviside step function. For large values of i[17], $a_i \to [(3\pi/2)(i+3/2)]^{2/3}$.

Using Eq. (16), the expression of the 1D electron concentration at low temperatures for the third order non-parabolicity of Kane can be written as

$$n_{1D} = \frac{2g_v}{\pi}\left(\frac{2m^*}{\hbar^2}\right)^{1/2} \sum_{n_x=1}^{n_{x\max}} \sum_{i=0}^{i_{\max}} \left[\zeta_3(E_F) - \left\{\frac{\hbar^2}{2m^*}\left(\frac{n_x\pi}{l_x}\right)^2 + a_i\left[\frac{\hbar eF_s[\zeta(E_F)]'}{\sqrt{2m^*}}\right]^{2/3}\right\}\right]^{1/2} \quad (17)$$

in which, E_F is the Fermi energy at the interface as measured from the edge of the conduction band in vertically upward direction.

Using Eq. (11) and proceeding in similar fashion, the electron dispersion relation, quantized subband energies, 1D DOS and n_{1D} for second order non-parabolicity of Kane for the present case can be respectively written as

$$\frac{\hbar^2 k_y^2}{2m^*} = E(1+\alpha E) - \frac{\hbar^2}{2m^*}\left(\frac{n_x\pi}{l_x}\right)^2 - a_i\left[\frac{\hbar eF_s(1+2\alpha E)}{\sqrt{2m^*}}\right]^{2/3} \quad (18)$$

$$E_{n,i}(1+\alpha E_{n,i}) = \frac{\hbar^2}{2m^*}\left(\frac{n_x\pi}{l_x}\right)^2 + a_i\left[\frac{\hbar eF_s(1+2\alpha E_{n,i})}{\sqrt{2m^*}}\right]^{2/3} \quad (19)$$

$$N_{1D}(E) = \frac{g_v}{2\pi}\left(\frac{2m^*}{\hbar^2}\right)^{1/2} \sum_{n_x=1}^{n_{x\max}} \sum_{i=0}^{i_{\max}} \left[(1+2\alpha E)\left\{E(1+\alpha E) - \frac{\hbar^2}{2m^*}\left(\frac{n_x\pi}{l_x}\right)^2 - a_i\left[\frac{\hbar eF_s(1+2\alpha E)}{\sqrt{2m^*}}\right]^{2/3}\right\}^{-1/2} \times H(E - E_{n,i})\right] \quad (20)$$

$$n_{1D} = \frac{2g_v}{\pi}\left(\frac{2m^*}{\hbar^2}\right)^{1/2} \sum_{n_x=1}^{n_{x\max}} \sum_{i=0}^{i_{\max}} \left[E_F(1+\alpha E_F) - \left\{\frac{\hbar^2}{2m^*}\left(\frac{n_x\pi}{l_x}\right)^2 + a_i\left[\frac{\hbar eF_s(1+2\alpha E_F)}{\sqrt{2m^*}}\right]^{2/3}\right\}\right]^{1/2} \quad (21)$$

For parabolic band, the electron dispersion relation, quantized subband energies, 1D DOS and n_{1D} can respectively be written as

$$\frac{\hbar^2 k_y^2}{2m^*} = E - \frac{\hbar^2}{2m^*}\left(\frac{n_x\pi}{l_x}\right)^2 - a_i\left[\frac{\hbar eF_s}{\sqrt{2m^*}}\right]^{2/3} \quad (22)$$

$$E_{n,i} = \frac{\hbar^2}{2m^*}\left(\frac{n_x\pi}{l_x}\right)^2 + a_i\left[\frac{\hbar eF_s}{\sqrt{2m^*}}\right]^{2/3} \quad (23)$$

$$N_{1D}(E) = \frac{g_v}{2\pi}\left(\frac{2m^*}{\hbar^2}\right)^{1/2} \times \sum_{n_x=1}^{n_{x\max}} \sum_{i=0}^{i_{\max}} \left[\frac{H(E - E_{n,i})}{\sqrt{E - \{(\hbar^2/(2m^*))(n_x\pi/l_x)^2 + a_i[\hbar eF_s/\sqrt{2m^*}]^{2/3}\}}}\right] \quad (24)$$

$$n_{1D} = \frac{2g_v}{\pi}\left(\frac{2m^*}{\hbar^2}\right)^{1/2} \sum_{n_x=1}^{n_{x\max}} \sum_{i=0}^{i_{\max}} \left[E_F - \left\{\frac{\hbar^2}{2m^*}\left(\frac{n_x\pi}{l_x}\right)^2 + a_i\left[\frac{\hbar eF_s}{\sqrt{2m^*}}\right]^{2/3}\right\}\right]^{1/2} \quad (25)$$

However, at higher temperature, the expression of 1D electron concentration for parabolic energy bands can be written following Eq. (24) as

$$n_{1D} = \frac{2g_v\sqrt{2\pi m^* k_B T}}{h} \sum_{n_x=1}^{n_{x\max}} \sum_{i=0}^{i_{\max}} [F_{-1/2}(\eta_1)] \quad (26)$$

where, $F_j(\eta)$ is the Fermi-Dirac integral[31] of order j and $\eta_1 \equiv (1/(k_B T)) \times [E_F - \{(\hbar^2/(2m^*))(n_x\pi/l_x)^2 + a_i[\hbar e F_s/\sqrt{2m^*}]^{2/3}\}]$.

It should be noted that Eqs. (18)–(21) and (22)–(25), in general are the special cases of the corresponding Eqs. (14)–(17). The nature of Eqs. (24) and (26) can also be compared as provided elsewhere.[32–33] Our analytical results for parabolic energy band model using Bohr-Sommerfeld's quantization technique are also in confirmation with the theoretical approach of Vasilopoulos et al.,[34] which signatures the compatibility of our mathematical formulation taking the third and the second order band non-parabolicity in QWFETs as considered in this paper.

The quantum gate capacitance (QGC) (C_G) per unit length in quantum wire field effect devices (QWFED) can be written in general as

$$\frac{1}{C_G} = \frac{1}{e}\frac{\partial v_G}{\partial n_{1D}} \tag{27}$$

in which, v_G is the applied gate voltage. It should be noted that at the inversion regime, the surface electric field at the interface and the 1D electron concentration in the triangular well can be related as

$$F_s = \frac{e n_{1D}}{\varepsilon_{sc} l_x} \tag{28}$$

The Gaussian distribution profile of the dopant atoms $N_D(z)$ from the interface can be written following[28] as

$$N_D(z) = \left(\frac{2N_D^{2D}}{\Delta z + s}\right)\sqrt{\frac{\log 2}{\pi}}\exp\left(-4\log 2\left(\frac{z+s}{\Delta z+s}\right)^2\right) \tag{29}$$

in which $N_D^{2D}$is the donor concentration and Δz is the full width at half maximum (FWHM) as measured from the centre of Gaussian distribution. It should be noted that the reason for taking the Gaussian distribution of the donor atoms is due to the incorporation of vertical diffusion of the delta function. Since, the doped cap layer being made of the same material as that of the substrate, contains a positive charge density eN_c from the donors. Thus, $\phi(z)$ can be solved using the one dimensional Poisson's equation as

$$\begin{aligned}\phi(z) = {} & \frac{-eN_c}{2\varepsilon_s}(z+d+s)^2 \\ & - \left[\frac{eN_D^{2D}}{\varepsilon_s}(z+d+s)\mathrm{erf}\left(\frac{-4d\log 2}{\Delta z+s}\right)\right] \\ & - \frac{en_{1D}}{l_x}\left(\frac{z}{\varepsilon_s} - \frac{d}{\varepsilon_d}\right) - \left(\frac{eN_D^{2D}(\Delta z+s)}{\varepsilon_d}\right) \\ & \times \left\{\frac{-4d\log 2}{\Delta z+s}\mathrm{erf}\left(\frac{-4d\log 2}{\Delta z+s}\right)\right. \\ & \left. + \frac{1}{\sqrt{\pi}}\left\{1 - \exp\left(-\left(\frac{4d\log 2}{\Delta z+s}\right)^2\right)\right\}\right\}\end{aligned} \tag{30}$$

in which, s, c and d are the thickness of the delta-doped layer, cap and the undoped spacer layer respectively as measured from the interface and *erf* is the error function.[27]

The gate voltage v_G may be written as

$$v_G = \frac{\mu_s - \mu_m}{e} \tag{31}$$

in which, μ_s and μ_m are the Fermi levels of the 1DEG and the metal respectively, where, all the energies and potentials being measured from the conduction band minimum of the inversion layer. The Schottky barrier at the gate-surface boundary pins the conduction band E_c at the barrier voltage V_b above the metal Fermi level μ_m, so that $\mu_m = -e\phi(-(c+d+s)) - V_b$ and thus,

$$\begin{aligned}\mu_m = e^2\Bigg\{ & \frac{N_c c^2}{2\varepsilon_s} - \frac{n_{1D}}{l_x}\left(\frac{c+s}{\varepsilon_s} + d\left(\frac{1}{\varepsilon_d} + \frac{1}{\varepsilon_s}\right)\right) \\ & + N_D^{2D}\mathrm{erf}\left(\frac{-4d\log 2}{\Delta z+s}\right)\left\{\frac{c}{\varepsilon_s} - \frac{4d\log 2}{\varepsilon_d}\right\} \\ & - \frac{N_D^{2D}(\Delta z+s)}{\varepsilon_d\sqrt{\pi}}\left[1 - \exp\left\{-\left(\frac{4d\log 2}{\Delta z+s}\right)^2\right\}\right]\Bigg\} - V_b\end{aligned} \tag{32}$$

Using Eqs. (31) and (32), the gate bias equation assumes the form

$$\begin{aligned}v_G = {} & \frac{E_F(n_{2D}) + \zeta(E_i)}{e} + \frac{V_b}{e} \\ & - e\Bigg\{\frac{N_c c^2}{2\varepsilon_s} - \frac{n_{1D}}{l_x}\left(\frac{c+s}{\varepsilon_s} + d\left(\frac{1}{\varepsilon_d} + \frac{1}{\varepsilon_s}\right)\right) \\ & + N_D^{2D} erf\left(\frac{-4d\log 2}{\Delta z+s}\right)\left\{\frac{c}{\varepsilon_s} - \frac{4d\log 2}{\varepsilon_d}\right\} \\ & - \frac{N_D^{2D}(\Delta z+s)}{\varepsilon_d\sqrt{\pi}}\left[1 - \exp\left\{-\left(\frac{4d\log 2}{\Delta z+s}\right)^2\right\}\right]\Bigg\}\end{aligned} \tag{33}$$

As the electrons starts to colonize the channel, the gate bias becomes the threshold voltage (v_T). In such a case, the band becomes flat in the substrate; and the spacer reduces the Fermi and subband energies to zero, leading to the expression of v_T as,

$$\begin{aligned}v_T = {} & \frac{V_b}{e} - e\left\{\frac{N_c c^2}{2\varepsilon_s} + N_D^{2D}\mathrm{erf}\left(\frac{-4d\log 2}{\Delta z+s}\right)\right. \\ & \times \left\{\frac{c}{\varepsilon_s} - \frac{4d\log 2}{\varepsilon_d}\right\} - \frac{N_D^{2D}(\Delta z+s)}{\varepsilon_d\sqrt{\pi}} \\ & \left.\times \left[1 - \exp\left\{-\left(\frac{4d\log 2}{\Delta z+s}\right)^2\right\}\right]\right\}\end{aligned} \tag{34}$$

Using Eqs. (17), (27) and (33), the 1D QGC can be written for the third order energy band model of Kane as

$$\begin{aligned}\frac{1}{C_G} = {} & \frac{1}{l_x}\left(\frac{c}{\varepsilon_{sc}} + \frac{d}{\varepsilon_d} + \frac{s}{\varepsilon_{sc}}\right) \\ & + \frac{1}{e^2}[P_1(i, n_x, E_F) + Q_1(i, E_F)]\end{aligned} \tag{35}$$

RESEARCH ARTICLE

in which,

$$P_1(i,n_x,E_F) \equiv \left\{\frac{g_v}{\pi}\left(\frac{2m^*}{\hbar^2}\right)^{1/2}\sum_{n_x=1}^{n_{x_{max}}}\sum_{i=0}^{i_{max}}\left\{\left[\zeta_3(E_F)-\frac{\hbar^2}{2m^*}\left(\frac{n_x\pi}{l_x}\right)^2 - \frac{2}{3}a_i\left[\frac{\hbar eF_s[\zeta_3(E_F)]'}{\sqrt{2m^*}}\right]^{2/3}\right]^{-1/2} \times\left[(\zeta_3(E_F))' - \frac{2}{3}a_i\left[\frac{\hbar eF_s}{\sqrt{2m^*}}\right]^{2/3}\frac{[\zeta_3(E_F)]''}{([\zeta_3(E_F)]')^{1/3}}\right]\right\}^{-1}\right\}$$

and $Q_1(i,E_F) \equiv (2e/3\varepsilon_s)a_i\left[\frac{\hbar e[\zeta_3(E_F)]'}{\sqrt{2m^*}}\right]^{2/3}(F_s)^{-1/3}$.

Using Eqs. (21), (27) and (33), the 1D QGC can be written for the second order energy band model of Kane as

$$\frac{1}{C_G} = \frac{1}{l_x}\left(\frac{c}{\varepsilon_{sc}}+\frac{d}{\varepsilon_d}+\frac{s}{\varepsilon_{sc}}\right) + \frac{1}{e^2}[P_2(i,n_xE_F)+Q_2(i,E_F)] \quad (36)$$

in which,

$$P_2(i,n_x,E_F) \equiv \left\{\frac{g_v}{\pi}\left(\frac{2m^*}{\hbar^2}\right)^{1/2}\sum_{n_x=1}^{n_{x_{max}}}\sum_{i=0}^{i_{max}}\left\{\left[E_F(1+\alpha E_F)-\frac{\hbar^2}{2m^*}\left(\frac{n_x\pi}{l_x}\right)^2 - \frac{2}{3}a_i\left[\frac{\hbar eF_s(1+2\alpha E_F)}{\sqrt{2m^*}}\right]^{2/3}\right]^{-1/2} \times\left[(1+2\alpha E_F) - \frac{2}{3}a_i\left[\frac{\hbar eF_s}{\sqrt{2m^*}}\right]^{2/3}\frac{2\alpha}{((1+2\alpha E_F))^{1/3}}\right]\right\}^{-1}\right\}$$

and $Q_2(i,E_F) \equiv (2e/3\varepsilon_s)a_i\left[\frac{\hbar e(1+2\alpha E_F)}{\sqrt{2m^*}}\right]^{2/3}(F_s)^{-1/3}$.

Using Eqs. (25), (27) and (33), the 1D QGC can be written for the parabolic energy band model of Kane as

$$\frac{1}{C_G} = \frac{1}{l_x}\left(\frac{c}{\varepsilon_{sc}}+\frac{d}{\varepsilon_d}+\frac{s}{\varepsilon_{sc}}\right)+\frac{1}{e^2}[P_3(i,n_x,E_F)+Q_3(i,E_F)] \quad (37)$$

in which,

$$P_3(i,n_x,E_F) \equiv \left\{\frac{g_v}{\pi}\left(\frac{2m^*}{\hbar^2}\right)^{1/2}\sum_{n_x=1}^{n_{x_{max}}}\sum_{i=0}^{i_{max}}\left[E_F-\left\{\frac{\hbar^2}{2m^*}\left(\frac{n_x\pi}{l_x}\right)^2 + a_i\left[\frac{\hbar eF_s}{\sqrt{2m^*}}\right]^{2/3}\right\}\right]^{-1/2}\right\}^{-1}$$

and $\quad Q_3(i,E_F) \equiv \frac{2e}{3\varepsilon_s}a_i\left[\frac{\hbar e}{\sqrt{2m^*}}\right]^{2/3}(F_s)^{-1/3}$

At higher temperatures, using Eq. (26), the 1D QGC for parabolic energy bands can be written as

$$\frac{1}{C_G} = \frac{1}{l_x}\left(\frac{c}{\varepsilon_{sc}}+\frac{d}{\varepsilon_d}+\frac{s}{\varepsilon_{sc}}\right) + \frac{1}{e^2}[P_4(i,n_xE_F)+Q_3(i,n_xE_F)] \quad (38)$$

where,

$$P_4(i,n_x,E_F) \equiv \left\{\frac{2g_v}{h}\left(\frac{2\pi m^*}{k_BT}\right)^{1/2}\sum_{n_x=1}^{n_{x_{max}}}\sum_{i=0}^{i_{max}}F_{-3/2}(\eta_1)\right\}^{-1}$$

2.3. Formulation of the Quantized Drain Current in III–V Delta Doped QWFETs Using Bohr-Sommerfeld's Quantization Rule in the Strong Inversion Regime Considering the Third, Second and First Order Band Non-Parabolicity

Assuming a linear relationship between the drain field (v_d) and the drain voltage (v_D) to be of the form as

$$F_d = F_s - \left(\frac{v_D}{c+d+s}\right) \quad (39)$$

The ballistic 1D drain current at low temperatures due to the positive and negative k-states using Eqs. (17), (21) and (25), following Natori's model,[6, 33] can be written as

$$I_+ = \frac{eg_v}{\pi\hbar}\sum_{n_x=1}^{n_{x_{max}}}\sum_{i=0}^{i_{max}}[E_{F_s}-E_{n,i}] \quad (40)$$

$$I_- = \frac{eg_v}{\pi\hbar}\sum_{n_x=1}^{n_{x_{max}}}\sum_{i=0}^{i_{max}}[E_{F_D}-E_{n,i}-ev_D] \quad (41)$$

in which, v_D is the applied drain bias and $E_{n,i}$ must be determined from Eqs. (15), (19) and (23) for each of the energy band models respectively.

Thus, the total 1D ballistic drain current in general for all the energy band models can be written as

$$I = I_+ - I_- \quad (42)$$

Figure 2 exhibits the distribution of the quantizing electric fields F_s and v_d throughout the channel interface. In the absence of the drain bias, the only field in the interface is F_s, while in the presence of a low drain bias, F_s and F_d are distributed right at the bottlenecks of the source and the drain respectively.

For a consistent solution of Eq. (42), it should be noted that at absolute zero temperature, all the drain states are occupied only if $E_{F_D}-E_{n,i}-ev_D > 0$, i.e., the upper limit of the drain bias must be in accordance with

$$v_D \le (E_{F_D}-E_{n,i})/e \quad (43)$$

However, at higher temperature, the upper limiting value of v_D must be determined by properly solving the coupled carrier statistic relation and the corresponding surface electric potential equation for each of the respective energy bands.

Also, while determining the Fermi energy from the 1D carrier degeneracy relations, the flux from the positive and negative k-states should be determined from the relation

$$n_{1D_+} = \frac{1}{2}n_{1D}\Big|_{E_{F_s}=E_F} \quad (44)$$

RESEARCH ARTICLE

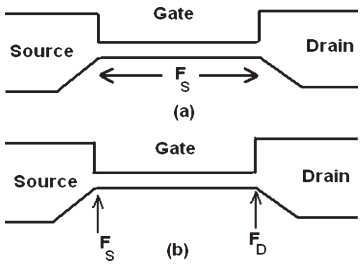

Fig. 2. The surface electric field at the bottlenecks of the ballistic QWFET in (a) the absence of drain bias and (b) the presence of the drain bias.

and

$$n_{1D_-} = \frac{1}{2} n_{1D}\Big|_{E_{F_D}=E_F-ev_D} \tag{45}$$

At higher temperature, using Eq. (42), the drain current for parabolic energy band model can be written in general as,

$$I = \frac{eg_v k_B T}{\pi\hbar}\left[\left\{\sum_{n_x=1}^{n_{x\max}}\sum_{i=0}^{i_{\max}}[F_0(\eta_+)]\right\} - \left\{\sum_{n_x=1}^{n_{x\max}}\sum_{i=0}^{i_{\max}}[F_0(\eta_-)]\right\}\right] \tag{46}$$

in which,

$$\eta_+ \equiv \frac{1}{k_B T}\left[E_{F_s} - \left\{\frac{\hbar^2}{2m^*}\left(\frac{n_x\pi}{l_x}\right)^2 + a_i\left[\frac{\hbar e F_s}{\sqrt{2m^*}}\right]^{2/3}\right\}\right] \quad \text{and}$$

$$\eta_- \equiv \frac{1}{k_B T}\left[E_{F_d} - \left\{\frac{\hbar^2}{2m^*}\left(\frac{n_x\pi}{l_x}\right)^2 + a_i\left[\frac{\hbar e F_d}{\sqrt{2m^*}}\right]^{2/3}\right\} - ev_D\right]$$

In this context, it should be noted that the ballistic 1D current in general depends on the band structural properties of the channel material through $E_{n,i}$, since this stands out as the lowest energy (quantized), which must have to be taken into account in determining the 1D DOS and thus the ballistic currents for such systems.

3. RESULT AND DISCUSSION

Using Table I and Eqs. (7), (8) and (9), in Figures 3 and 4, we have plotted the subband energy dispersion relation for the third and second order band non-parabolicity of Kane, together with the parabolic energy band respectively for the present system. It can be inferred that the contribution due to both type of band non-parabolicity becomes extremely significant for the high energy electrons. A self-consistent result for the subband energies derived from the Poisson-Schrödinger's (PS) equation and that of Bohr-Sommerfeld's quantization integral can be clearly seen by comparing the numerical values of the electron energies of the 1D DOS as shown in Figures 5–7 for all types of dispersion relations. It may be noted that a similar self-consistent result between the PS equation and the Bohr-Sommerfeld's quantization integral rule for a

Table I.

InAs[11]	$E_g = 0.36$ eV, $\Delta = 0.43$ eV and $m^* = 0.026m_0$, $g_v = 1$ and $\varepsilon_{sc} = 12.25\varepsilon_0$
$In_{1-x}Ga_xAs$[42, 43]	$E_g = (0.4105 + 0.6337x + 0.475x^2)$ eV, and $m^* = (0.023 + 0.037x + 0.003x^2)m_0$
Cap thickness	10 nm
Dopant thickness	5 nm
Spacer Thickness	5 nm
N_D^{2D}	5×10^{14} m^{-2}
Δz	30 Å

quasi two-dimensional non-parabolic electron gas system in inversion layer has also been verified by King et al.[22]

The 1D DOS for the present system also exhibits a set of composite oscillations as function of electron energy by taking all the aforementioned energy band models. Due to the presence of the lateral (structural) and a vertical (electrical) quantization, the electrons in such systems are constrained to remain confined in both directions. The lowest energy state of the confined electrons can be determined by their respective band structures and the quantum integrals n_x and i. Eqs. (15), (19) and (23) exhibits the discrete subband energies of the electrons obeying the three, two and the parabolic energy bands respectively. The composite oscillations as shown in the said figures are also similar in nature for a 1D trigate SOI MOSFETs,[32] where there is only an electrical confinement.

Using Eqs. (17), (35); (21), (36) and (25), (37) together with Eq. (33), in Figure 8, we have plotted the QGC per unit length as function of the surface electric field and the gate bias respectively at $T = 0$ K for InGaAs | InAs δ-doped QWFED, whose 1DEG follows the third, second and the parabolic energy band models of Kane respectively. The relative shift of the QGC clearly exhibits the significant dependence of the same on the spectrum constants and the lateral dimension of the effective channel length. The application of high values of electric field on

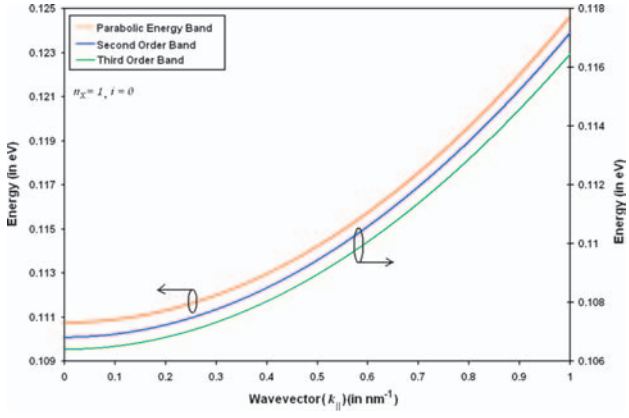

Fig. 3. Plot of the subband energies taking $n_x = 1$ and $i = 0$ as function of wave vector along y-direction in accordance with the self-consistent PS equation for the δ-doped InGaAs/InAs ballistic QWFED whose channel carriers obeys parabolic, second and third order energy band models.

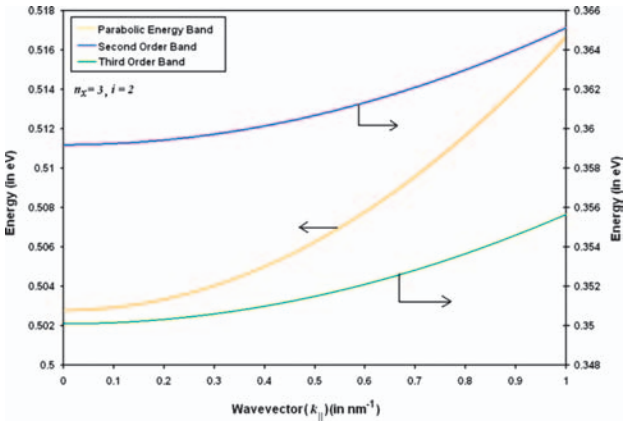

Fig. 4. Plot of the subband energies $n_x = 3$ and $i = 2$ as function of wave vector along y-direction in accordance with the self-consistent PS equation for the δ-doped InGaAs/InAs ballistic QWFED whose channel carriers obeys parabolic, second and third order energy band models.

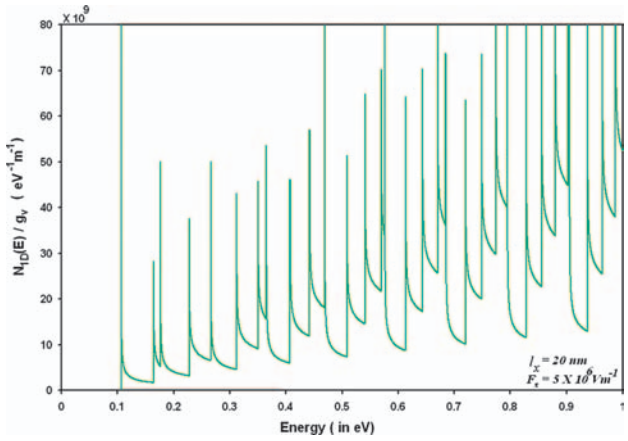

Fig. 6. Plot of the normalized 1D DOS as function of electron energy in the strong inversion regime for δ-doped InGaAs/InAs ballistic QWFED whose channel carriers obeys second order energy band model using the Bohr-Sommerfeld's rule.

the channel region results the formation of a large number of electric subbands, which signatures the vertical confinement of the motion of the carriers and hence the quantized Fermi energies. This severe discontinuity in the 1D DOS changes the smooth variation of the gate capacitance into a discrete behavior. The magnitude of the QGC is significantly enhanced by the contribution of subbands due to both electrical and structural counterparts respectively. It should be noted that the value of the QGC in QWFEDs can be considerably less than that of the corresponding cases of bulk MOS devices. This is due to the fact that the 1D DOS can be greatly reduced by the application of gate bias and the lateral dimension. This results in lowering of the net amount of charge at the interface and hence lowering of the QGC. The influence of quantum confinement is immediately apparent from Figure 8, since, QGC depends strongly on the quantized energies of the 1DEG, which is in high direct contrast with their respective bulk devices.

With higher values of the interface electric field, the carrier degeneracy in the strongly inverted channel increases thereby increasing QGC. The oscillatory dependences are due to the crossing over of the Fermi level by the quantized levels. For each coincidence of such levels with the Fermi level, there would be a discontinuity in the density-of-states function resulting in a sudden jump in magnitude. Composite oscillations have also been predicted for the QGC in the present system. Careful experiments for the 1D rectangular transistors may uncover new physical phenomena in this context. However, as one increases the gate bias, next set of energy levels due to the electrical and structural counterparts starts filling up from the beginning, which pulls down the QGC. The numerical values of the QGC vary widely for the three types of energy dispersion relation, and are determined by the constants of the energy spectra and the quantum integers. It should be noted that the height of step size and the rate of increment

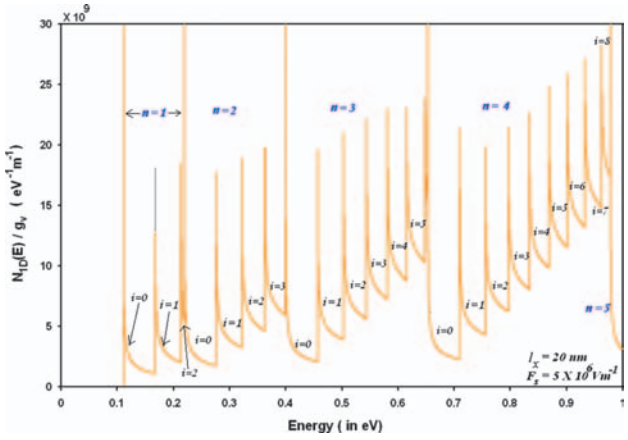

Fig. 5. Plot of the normalized 1D DOS as function of electron energy in the strong inversion regime for δ-doped InGaAs/InAs ballistic QWFED whose channel carriers obeys parabolic energy band model using the Bohr-Sommerfeld's rule.

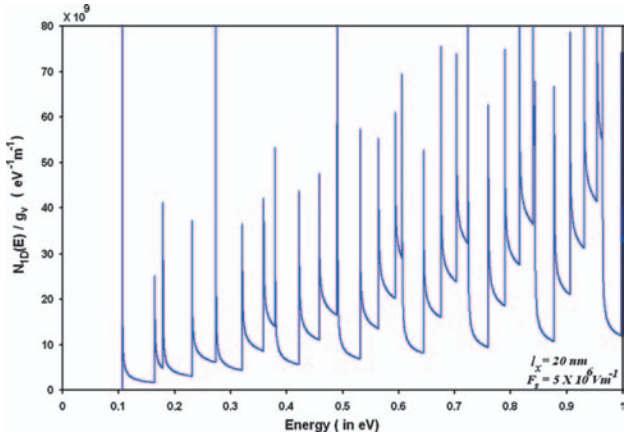

Fig. 7. Plot of the normalized 1D DOS as function of electron energy in the strong inversion regime for δ-doped InGaAs/InAs ballistic QWFED whose channel carriers obeys the third order energy band model using the Bohr-Sommerfeld's rule.

RESEARCH ARTICLE

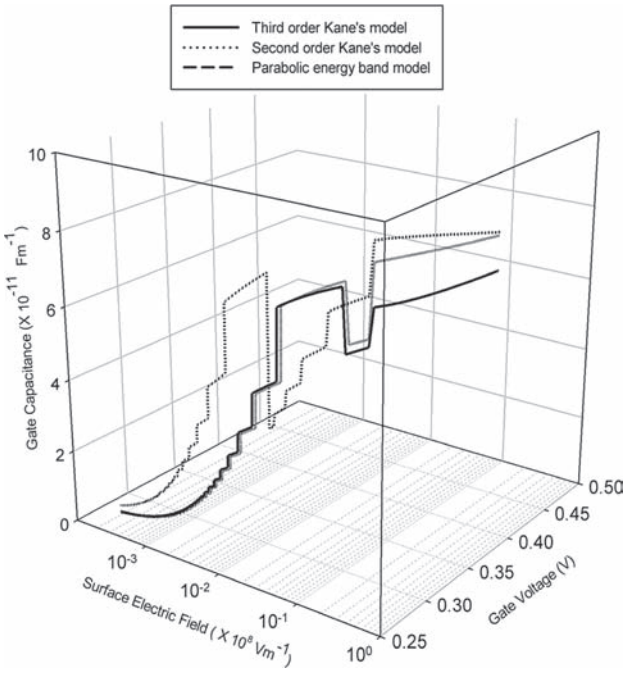

Fig. 8. Plot of the Quantum Gate Capacitance as function of surface electric field at the interface and applied gate voltage in the strong inversion regime for δ-doped InGaAs/InAs ballistic QWFED whose channel carriers obeys the third, the second and the parabolic energy band model of Kane.

and decrement are totally dependent on the band structure of the 1DEG.

Using Eqs. (39)–(45), in Figures 9 and 11, we have plotted the drain current dependency on the gate and the drain bias respectively. The Figure 10 exhibits the enlarged view of the same at low gate and drain bias. From Eqs. (40)–(42) and (46), it can be noted that the inclusion of the ballistic transport readily removes the dependency of the

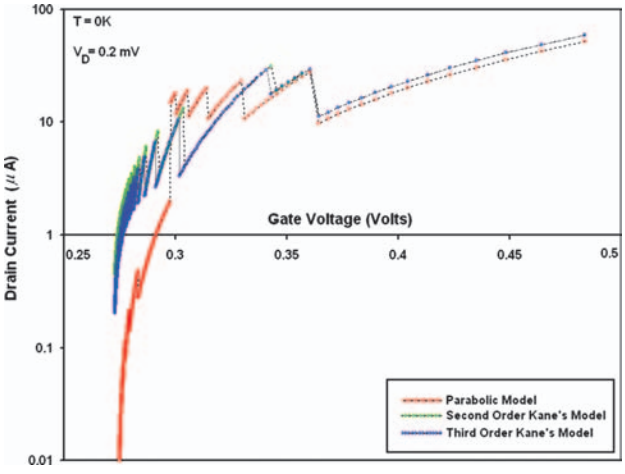

Fig. 9. Plot of the 1D ballistic quantized drain current as function of gate voltage at low drain bias for δ-doped ballistic InGaAs/InAs QWFET accordance with the third, second and the parabolic energy band model of Kane.

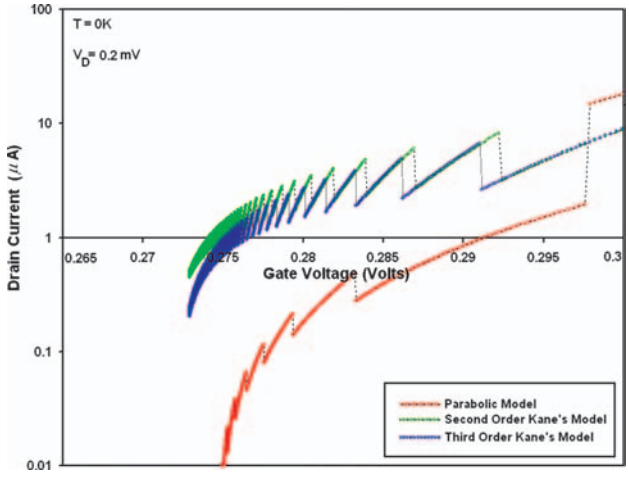

Fig. 10. Enlarge view of the 1D ballistic quantized drain current as function of low gate bias voltage for all the cases of Figure 9.

drain current on the channel length of the QWFETs. In the absence of the drain voltage, the negative k-states carrier degeneracy converges to that of the positive k-state degeneracy. For a fixed F_s, as one increases the drain bias from zero, F_d decreases (Eq. (39)), which simultaneously reduces the drain Fermi energy such that

$$\zeta(E_{F_d}) \geq \left\{ \frac{\hbar^2}{2m^*}\left(\frac{n_x\pi}{l_x}\right)^2 + a_i\left[\hbar e F_d[\zeta(E_{F_d})]'/\sqrt{2m^*}\right]^{2/3} \right\}$$

thereby tending I to a saturated value I_s. It can also be seen that the expressions of I can be determined from the corresponding 1DEG carrier degeneracy relation for a particular band structure in the presence of a chosen very high gate electric field at the source bottleneck such that carrier degeneracy at the order of 10^{14} m^{-2} is achieved at the interface.[6, 19, 26, 35] In other words, the determination of I demands the knowledge of Fermi energy of the carriers at the interface as measured from the conduction band

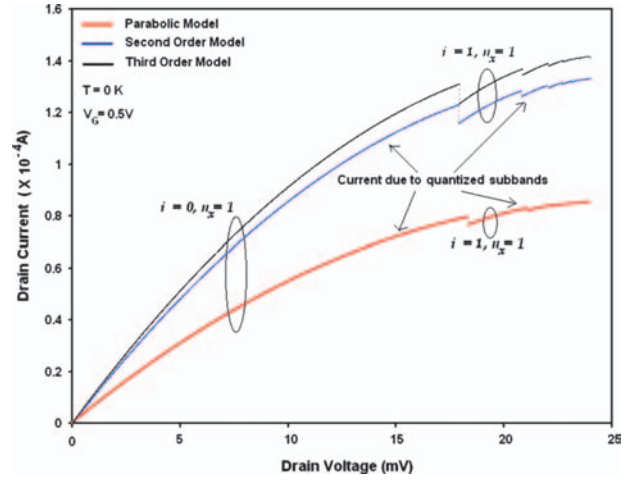

Fig. 11. Plot of the 1D ballistic quantized drain current as function of low drain bias for δ-doped InGaAs/InAs ballistic QWFET in accordance with the three, the two and the parabolic energy band model of Kane.

RESEARCH ARTICLE

minima in the vertically upward direction, which can in turn be known by solving the carrier degeneracy relation for a particular value of surface electric field at the inversion layer bottlenecks both at the source and the drain end. The expression of the gate voltage for a chosen F_s can also be determined by solving analytically the corresponding potential function and has been described for a 2DEG system.[23]

Similar oscillations in drain current as function of both the gate and the drain bias at low temperatures for different 1D ballistic nano-transistors has also been experimentally verified.[3–5, 32] For the present system, the composite oscillations of the drain current is clearly been sought out. It appears that there is a significant relative shift in the magnitude of the drain current between the parabolic and non-parabolic energy bands. It also appears from all the figures that the discrimination between the second and third order energy bands are relatively low, but, both have significant deviation from the parabolic energy band. The drain bias has been taken to be very low incorporating the consistency with Eq. (43). At much higher temperature, the maximum drain bias value can be determined by properly solving the coupled electron statistics and the corresponding electric potential function, both at the drain and the source bottle necks, for each of the respective energy bands.

It should be noted that the magnitude of I in inversion layers can be extremely large depending on the amount of degeneracy and the number of subbands present at the interface. In case of lowest occupied subband, I can be less, since, as the gate bias affects the 1D DOS, reducing the states. This results in lowering of the net amount of charge at the interface and hence lowers I. The contribution of large number of the subbands aids to enhance the drive current I. In addition, as the spacer layer in such transistors spatially isolates the impurities and the 1DEG, the mobility can be extremely large leading to negligible ionized impurity scattering. At low temperatures, phonon scattering minimizes and thus tending to a more ballistic transport condition.

In Figure 12, we have plotted the quantized channel conductance (QCC) as function of applied gate voltage in the presence of a low drain bias at low temperature for all the energy band models. The inclusion of the structural and electrical subbands, results a composite oscillation in QCC. It can also be seen that the peaks of the QCC for all the bands takes a jump of $2e^2 g_v/h$.

Due to a condensed paper presentation, we have not provided the detailed analyses of the sub-threshold slope for degenerate 1D QWFETs incorporating the band non-parabolicity and composite subbands in this context. However, from Figures 9–11, one can estimate the same with the magnitudes of the on and off currents. Furthermore, the influences of the composite quantization and defect centers due to the alloy composition, x, (DX centers) on

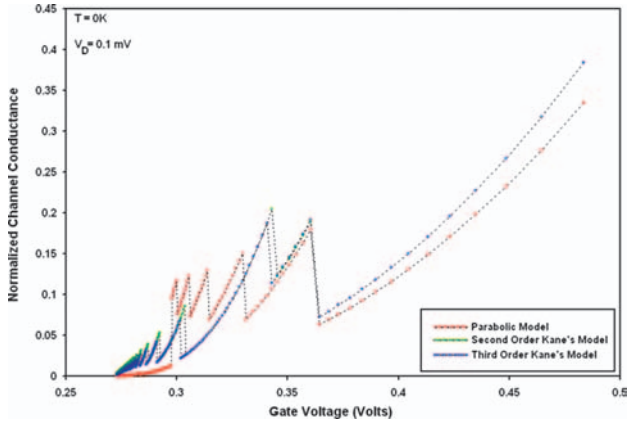

Fig. 12. Plot of the 1D ballistic normalized quantized channel conductance as function of gate voltage for δ-doped InGaAs/InAs ballistic QWFET accordance with the two and the three band model of Kane for two different values of gate voltage.

threshold voltage have been neglected which can affect the 1D QGC and the 1D ballistic drain currents.[36–37] Such incorporation would certainly enhance the accuracy of our results on the threshold voltage. Our generalized theoretical results on the ballistic 1D drain current can be compared with the available experimental data for relative comparison.[3–5, 32, 38, 39] It may be noted that the ballistic condition can also be applied at *sub-50* nm scaled devices.[7] Keeping this in view, we have neglected the back-scattering of the carriers in the channel. However, since the effective channel length being in few tens of nanometers, the omission of this type of scattering will not appreciably change both the qualitative and quantitative nature of the ballistic expressions as derived in this paper. Also, while deriving the results using Bohr-Sommerfeld's rule, we have not used the available technique[40] in the literature to calculate the density-of states, since from the carrier dispersion relation, one can obtain the DOS, but the DOS technique as used in literature[40] cannot provide the carrier dispersion relation. Thus, our study is more fundamental than those existing in the literature, since the Boltzmann transport equation, which controls the study of the charge transport properties of semiconductor devices, can be solved if and only if the corresponding $\mathbf{E}-\mathbf{k}$ dispersion relation is known. The electrical potential well at the interface has been assumed to be approximated by a linear triangular well, which however, introduces some errors, such as, negligence of the free charge contribution to the potential. This kind of approach is reasonable if there are only a few charge carriers in the inversion layer, but is responsible for an overestimation of the splitting when the inversion carrier density exceeds that of the depletion layer. This approximation will not introduce significant error since, for actual calculations, one need to derive analytical solutions to solve the coupled PS equation self-consistently, which is a formidable problem for the present generalized system due to the non-availability

RESEARCH ARTICLE

of the proper analytical techniques, without exhibiting a widely different qualitative behavior.[26]

It should be noted that the usual methods in determining the ballistic properties of nano-transistors as available in the literature does not contain any quantum effects in general and are based on a homogeneous electron gas in a slowly varying potential without any discrete energy levels providing a maximum of the DOS at the interface where the band bending is greatest and where an abrupt interface barrier occurs. Since, in actual case, the density approaches zero as shown in Figures 5, 6 and 7 at the interface, which leads to the conclusion that the results become extremely wrong for stronger inversion regime.[14] For a compact modeling of the complex analytical formulation of the 1D QGC and 1D drain current for III–V QWFETs, the 1D DOS and 1D carrier degeneracy under a linear triangular potential well approximation under higher order band non-parabolicity by using the Bohr-Sommerfeld's rule as formulated in this paper can be suitable for a more generalized expressions. In the absence of band non-parabolicity, and considering only one filled subband, all the ballistic equations gets readily transformed to well-known results as derived elsewhere,[24, 33] which proves the mathematical compatibility of our overall results.

It may be remarked that, in recent years, the carrier statistics of III–V materials have been extensively studied, yet, the influence of 1DEG and band non-parabolicity on ballistic drain current for QWFETs have been less investigated by considering the inclusion of composite subbands. We wish to note that we have not considered the hot electron and many body effects in this simplified theoretical formalism due to the lack of proper analytical techniques in literature for including them in the present system. Our simplified model will be useful for the purpose of comparison when methods for tackling the formidable problem after inclusion of such effects for the present generalized systems would appear. The inclusion of the aforesaid effects would certainly increase the accuracy of our results, although the qualitative features of the drain current as discussed here would not change in the presence of the aforementioned effects. In order to keep the presentation brief, we have not considered other types of optoelectronic materials as channel material. The analytical methodologies as formulated in this paper can be used to predict the 1D ballistic behavior of other III–V QWFETs like AlGaAs/GaAs,[4] InAs/InP.[5] Since the band gap of these optoelectronic materials can be varied over a wide range by adjusting the alloy composition,[41] the corresponding case studies can uncover interesting physical phenomena. Besides, the influence of energy band models and the various band constants on the 1D ballistic drain current for different QWFETs made of groups of II–VI, IV–VI, etc. can also be estimated from our theoretical formulations.

4. CONCLUSIONS

We have presented a simplified yet analytic expressions of few ballistic properties of delta-doped III–V QWFETs whose channel electrons obey the third, second and first order energy band non-parabolicity using Bohr-Sommerfeld's quantization rule in strong inversion layers. A self-consistent numerical solution for complete subband structures using Poisson's-Schrödinger's equation and Bohr-Sommerfelds's rule for the said system has clearly sought out. The lateral (structural) and vertical (electrical) quantization predicts the composite oscillations in one-dimensional density-of-states function, quantum gate capacitance, ballistic drain current and quantum channel conductance, which agrees well with the similar experimental facts. Due to the negligible amount of ionic and phonon scattering, the drain current in such systems has significant high values. The expressions of all the ballistic properties for the present systems obeying nonlinear energy relations agree well to the corresponding relations of parabolic model when the band non-parabolicity disappears. The theoretical results as given here would be useful in analyzing various other physical and experimental facts[1, 26] related to this phenomenon. Finally, it may be concluded that this theory can also be used to investigate the drain current variation, gate capacitances, Burstien Moss shift, the effective electron mass, the specific heat and other different transport coefficients of modern ultrathin film semiconductor devices operated under the influence of external photon field.

Acknowledgment: The author Sitangshu Bhattacharya is grateful to the Department of Science and Technology, India, for sanctioning the project and the fellowship under "SERC Fast Track Proposal of Young Scientist" scheme-2008–2009, having the sanction number SR/FTP/ETA-37/08 under which this research paper has been completed.

References

1. M. Cahey and S. Bandhopadhyay, *IEEE Potentials*, 12, 18 **(1993)**.
2. http://www.itrs.net/Links/2007ITRS/2007_Chapters/2007_ERD.pdf.
3. K. Yoh, A. Nishida, and M. Inoue, *IEEE, Trans. Electron. Dev.* 40, 2134 **(1993)**.
4. J. Christen, E. Kapon, M. Grundmann, D. M. Hwang, M. Joschko, and D. Bimberg, *Phys. Stat. Sol. (b)* 173, 307 **(1992)**.
5. T. Angelova, A. Cros, A. Cantarero, D. Fuster, Y. González, and L. González, *J. Appl. Phys.* 104, 033523 **(2008)**.
6. K. Natori, *J. App. Phys.* 76, 4879 **(1994)**.
7. J. Wang and M. Lundstrom, *IEEE, Trans. Electron. Dev.* 50, 1604 **(2003)**.
8. K. Yoh, H. Taniguchi, K. Kiyomi, M. Inoue, and R. Sakamoto, *IEDM '91. Tech. Digest.* **(1991)**, pp. 813–816.
9. K. Yoh and S. Takabayashi, *Phys. Stat. Sol. (b)* 204, 259 **(1997)**.
10. E. O. Kane, *J. Phys. Chem. Solids* 1, 249 **(1957)**.
11. B. R. Nag, Electron Transport in Compound Semiconductors, Springer-Verlag **(1980)**.

RESEARCH ARTICLE

12. S. Bhattacharya, R. Sarkar, D. De, S. Mukherjee, S. Pahari, A. Saha, S. Roy, and K. P. Ghatak, *J. Comput. Theor. Nanosci.* 6 **(2008)**, in the press.
13. T. Fiedler, Dissertation A, Technische Hochschule Ilmenau **(1984)**.
14. H. Ubensee, G. Paasch, and J.-P. Zollner, *Phys. Stat. Sol. (b)* 134, 367 **(1986)**.
15. H. Übensee, G. Paasch, and J.-P. Zöllner, *Phys. Rev. B* 39, 1955 **(1989)**.
16. G. A. Antcliffe, R. T. Bate, and R. A. Reynolds, Physics of semimetals and narrow-gap semiconductors, *Proc. Int. Conf.*, edited by D. L. Carter and R. T. Bate, Pergamon Press, Oxford **(1971)**, pp. 499–503.
17. G. Paascht, T. Fiedler, M.Kolar, and I. Bartos, *Phys. Stat. Sol. (b)* 118, 641 **(1983)**.
18. J.-P. Zollner, H.Ubensee, G. Paascht, T. Fiedler, and G. Gobsch, *Phys. Stat. Sol. (b)* 134, 837 **(1986)**.
19. J.-P. Zollner and G. Paasch, *Phys. Stat. Sol. (b)* 151, 145 **(1989)**.
20. K. P. Ghatak, N. Chattopadhyay, and M. Mondal, *Appl. Phys. A* 48, 365 **(1989)**.
21. K. P. Ghatak and S. Biswas, *J. Vac. Sc. Tech. B* 7, 104 **(1989)**.
22. P. D. C. King, T. D. Veal, and C. F. McConville, *Phys. Rev. B* 77, 125305 **(2008)**.
23. S. Bhattacharya, S. S. Dan, and S. Mahapatra, *J. Appl. Phys.* 104, 074304 **(2008)**.
24. J. P. Collinge, FinFET and Other Multigate Transistors, edited by J. P. Collinge, Springer Series on Integrated Circuits and Systems, USA **(2008)**, and the references cited their in.
25. V. V. Mitin, V. A. Kochelap, and M. A. Stroscio, Quantum Heterostructures: Microelectronics and Optoelectronics, Cambridge University Press **(1999)**.
26. T. Ando, A. B. Fowler, and F. Stern, *Rev. Mod. Phys.* 54, 437 **(1982)**.
27. M. Abramowitz and I. A. Stegun, Handbook of Mathematical functions, Verlag, Harry, Deutch, Franckfurt a.M. **(1984)**.
28. A. Ben Jazia, H. Mejri, H. Maaref, and K. Souissi, *Semicond. Sci. Technol.* 12, 1388 **(1997)**.
29. B. R. Nag, Physics of Quantum Well devices, Kluwer Academic Publishers **(2002)**.
30. R. Landauer, *Phil. Mag.* 21, 863 **(1970)**.
31. J. S. Blackmore, Semiconductor Statistics, Pergamon Press, Oxford-London-New York-Paris **(1962)**.
32. J. P. Colinge, *J. Solid-State Electron.* 51, 1153 **(2007)**.
33. M. Lundstrom and J. Guo, Nanoscale Transistors, Springer **(2006)**.
34. P. Vasilopoulos and F. M. Peeters, *Phys. Rev. B* 40, 10079 **(1989)**.
35. E. H. Hwang and S. Das Sarma, *Phys. Rev. B* 77, 235437 **(2008)**.
36. G. Chindalore, S. A. Hareland, S. Jallepalli, A. F. Tasch, Jr., C. M. Maziar, V. K. F. Chia, and S. Smith, *IEEE, Electron Dev. Lett.* 18, 206 **(1997)**.
37. A. Chandra and M. C. Foisy, *IEEE, Trans. Electron Dev.* 38, 1238 **(1991)**.
38. K. Yoh, H. Taniguchi, K. Kiyomi, M. Inoue, and R. Sakamoto, *IEDM Tech. Digest* **(1991)**, pp. 813–816.
39. A. F. J. Levi, R. J. Spah, and J. H. English, *Phys. Rev. B* 36, 9402 **(1987)**.
40. J. N. Schulman and Y. C. Chang, *Phys. Rev. B* 24, 4445 **(1981)**.
41. J. Singh, Semiconductor Optoelectronics: Physics and Technology, Mc Graw Hill **(1995)**.
42. K.-H. Goetz, D. Bimberg, H. Jurgensen, J. Selders, A. V. Solomonov, G. F. Glinskii, and M. Razeghi, *J. Appl. Phys.* 54, 4543 **(1983)**.
43. T. P. Pearsall, GaInAsP Alloy Semiconductors, John Wiley and Sons, **(1982)**.

Received: 22 November 2008. Accepted: 6 January 2009.